Time-temperature equivalence in a PVA dual cross-link self-healing hydrogel

Mincong Liu, Jingyi Guo, Chung-Yuen Hui, Costantino Creton, Tetsuhara Narita, Alan Zehnder

Time-temperature equivalence in a PVA dual cross-link self-healing hydrogel

Mincong Liu, Jingyi Guo, Chung-Yuen Hui, Costantino Creton, Tetsuhara Narita, and Alan Zehnder

Citation: Journal of Rheology **62**, 991 (2018); doi: 10.1122/1.5029466
View online: https://doi.org/10.1122/1.5029466
View Table of Contents: https://sor.scitation.org/toc/jor/62/4
Published by the The Society of Rheology

Time-temperature equivalence in a PVA dual cross-link self-healing hydrogel

Mincong Liu,[1] Jingyi Guo,[1] Chung-Yuen Hui,[1] Costantino Creton,[2,3] Tetsuhara Narita,[2,3] and Alan Zehnder[1,a)]

[1]*Sibley School of Mechanical and Aerospace Engineering, Field of Theoretical and Applied Mechanics, Cornell University, Ithaca, New York 14853*

[2]*Laboratoire Sciences et Ingénierie de la Matière Molle, PSL Research University, UPMC Univ Paris 06, ESPCI Paris, CNRS, 10 rue Vauquelin, 75231 Paris Cedex 05, France*

[3]*Global Station for Soft Matter, GI-CoRE, Hokkaido University, Sapporo 060-0808, Japan*

(Received 14 March 2018; final revision received 31 May 2018; published 5 July 2018)

Abstract

Hydrogels consisting of permanent chemical bonds plus transient physical bonds are known to have self-healing properties, high toughness, and to be highly viscoelastic. These mechanical responses derive from the ability of the physical bonds to break and reform during deformation. The rate of bond breaking and reformation is found experimentally to be independent of stress but is expected to depend on temperature. Using a poly(vinyl alcohol) hydrogel with chemical and physical cross links, the temperature dependence of the mechanical response is measured using large strain load/unload tension tests and torsional rheometry for temperatures from 13 to 50 °C. The rheometry data show that time-temperature superposition can be used to condense the data to a master curve. It is found that allowing the model parameters to be temperature dependent, a previously developed constitutive model fits the tension and rheometry data well. Horizontal (time) and vertical (amplitude) shift factors calculated directly from the rheometer test data and from tension test data agree well with each other showing that the constitutive model describes the mechanical behavior well over the temperature range explored and that the material closely follows simple time-temperature superposition. © *2018 The Society of Rheology*.
https://doi.org/10.1122/1.5029466

I. INTRODUCTION

A hydrogel is essentially a network of crosslinked polymer chains swollen in water. An issue with conventional covalently crosslinked hydrogels is that they are too brittle to use in load bearing structures. The area of hydrogel mechanics has advanced rapidly since several new synthetic routes of mechanical reinforcement of hydrogels have been developed [1–4]. Gong *et al*. introduced the concept of sacrificial bonds: They demonstrated that it is possible to make stiff and tough hydrogels with a double network structure by breaking internal sacrificial bonds [1,5]. In these gels having interpenetrated networks, the first network is brittle as it is highly cross-linked and swollen (thus dilute and stretched) and serves as a sacrificial network. The second network is loosely cross-linked and highly extensible. During mechanical loading, the first network bears most of the load and undergoes progressive irreversible damage, while the second network prevents the formation and growth of macroscopic cracks. Because the first network is chemically cross-linked and is irreversibly broken, this gel does not fully recover its original state after damage [5]. Nevertheless, such gels have a good resistance to crack propagation in fatigue, as shown by the recent works of Suo and coworkers [6].

Recently, several research groups have used noncovalent transient interactions as sacrificial bonds to synthesize highly stretchable and tough hydrogels [4]. These physical interactions are reversible and can break and reform. These gels exhibit time dependent viscoelastic behavior and recover to their original state upon load removal. Sun *et al*. [4] reported tough physically crosslinked polyampholyte hydrogels having ionic bonds. It was claimed that the polymer network is formed by self-healing weak bonds as well as strong bonds which maintain the network integrity over a sufficiently long time scale [7]. For the interested readers, two reviews on the relative merits of these different hydrogels have recently been published [8,9].

Varying the temperature changes the breaking and reattaching rates of the physical bonds. Thus, for hydrogels with transient physical bonds, temperature will have significant effects on the mechanical response. For many polymers, the relation between strain rates and temperature is found to obey the time-temperature superposition principle (TTS). Since time dependent gels have only recently been introduced, there are few studies on the effects of temperature and loading rate on the mechanical behavior of these gels. Recently, Sun *et al*. [10] showed that it was possible to use vertical and horizontal shift factors to collapse small strain rheology data onto a master curve for polyampholyte hydrogels. Further, they measured the hysteresis from uniaxial cyclic tests carried out at moderately large strains. They found that the *hysteresis* from tests with different stretch

a)Author to whom correspondence should be addressed; electronic mail: Atz2@cornell.edu

rates and temperatures can be collapsed onto a master curve using the same shift factors obtained from the rheology.

The goal of the current work is to build on prior models to develop a complete, three-dimensional (3D), constitutive model that incorporates the effect of temperature on the rate of breaking/healing of physical bonds as well as on other physical parameters. With this model, one will be able to compute the mechanical response over a range of stretch rates and temperatures and to directly compare data from constant strain rate, large stretch tension tests to cyclic, torsional rheology, and small strain tests.

In this paper, we study the effects of temperature and loading rate on the mechanical response of poly(vinyl alcohol) (PVA) dual cross-link hydrogel with PVA chemically crosslinked by glutaraldehyde and physically crosslinked by borate ions [11]. Although this gel has a lower resistance to fracture in comparison to the polyampholyte gels developed by Gong *et al.* [1], it has a well-defined simple chemical structure with only one type of physical crosslink between PVA chains, thus providing an ideal platform for understanding the interplay between microscopic bond kinetics and macroscopic mechanics. In addition, we have previously developed a 3D constitutive model which combines the finite strain elasticity of elastomers with the kinetics of bond breaking and reattachment [12–14] and demonstrated that our model can accurately capture the behavior of both uniaxial tension and shear (cyclic, small strain torsion) tests with complex loading histories at room temperature. This constitutive model developed here enables us to compare data obtained from rheometer tests at different temperatures directly with data obtained from uniaxial, constant stretch rate loading/unloading tests performed at different loading rates and temperatures.

The outline of this paper is as follows: In Sec. II, we present the experimental procedure and the test setup for temperature control. The experimental results from uniaxial tension tests at different temperatures are presented in Sec. III along with the comparison to the predictions of our constitutive model. Results of rheology tests at different temperatures are presented in Sec. IV. These results show that the PVA gel closely obeys the TTS with a horizontal (time) and vertical (amplitude) shift factors. This section also gives a detailed discussion on the relation between parameters in our constitutive model and the shift factor. Section V summarizes the findings.

II. EXPERIMENTS

A. Material preparation

The dual-crosslink PVA hydrogels were prepared by incorporating borate ions in a chemically cross-linked PVA gel. Details of synthesis are provided in previous works [11,15]. Here, we briefly summarize the procedure. We first made the chemically cross-linked gel by mixing a glutaraldehyde solution into a PVA solution at $p\mathrm{H} = 1.4$, adjusted by hydrochloric acid (HCl). The PVA concentration in the solution was 12%, and the molar ratio of chemical cross-linker and PVA monomers was 1:500. The solution was then injected into a mold. After 24 h, the chemically cross-linked gel was removed from the mold and washed with plenty of water to neutralize the *p*H. Then, the chemical gel was soaked in a NaCl/Borax solution (Borax, 1 mM/l; NaCl 90 mM/l) for 3 days. Infusion of the ionic solution into the gel causes physical bonds to form. Once the NaCl/Borax soaking was completed, the samples were stored in the same solution for up to 2 weeks prior to testing. Two batches of material were used, one for the large strain tension tests and the other for the small strain rheology tests. Despite minor batch to batch variation, model parameters obtained from large strain tests of the first batch result in a model that fits the rheology data from the second batch well indicating that we are synthesizing consistent materials and demonstrating the robustness of the model.

B. Uniaxial tension tests

We performed uniaxial tensions tests on the hydrogel specimens at different loading rates and temperatures. The tests were performed using a custom built tensile tester. Translational motion was provided by a Zaber X-LSM200A-E03 translational stage. The load was measured by an Interface SMT1-1.1 load cell (4.9 N capacity) and displacement by an OMEGA LD620 linear variable displacement transducer. The load and displacement signals were recorded using a Keithley Model 2701 multiplexing digital voltmeter at rates of 25 pairs of data per second. During the tests, the hydrogel samples were immersed in mineral oil to prevent drying. The oil exerts a buoyant force on the grips. This force was experimentally calibrated and subtracted from the measured load to avoid systematic error.

The temperature of the test environment was maintained by a custom built system which is schematically shown in Fig. 1. The system is insulated by gluing insulation foam to the outer surfaces of the acrylic oil container. Prior to testing, we preheated the oil and poured the preheated oil into the tank. Two low power immersion heaters (total power of 15 W)

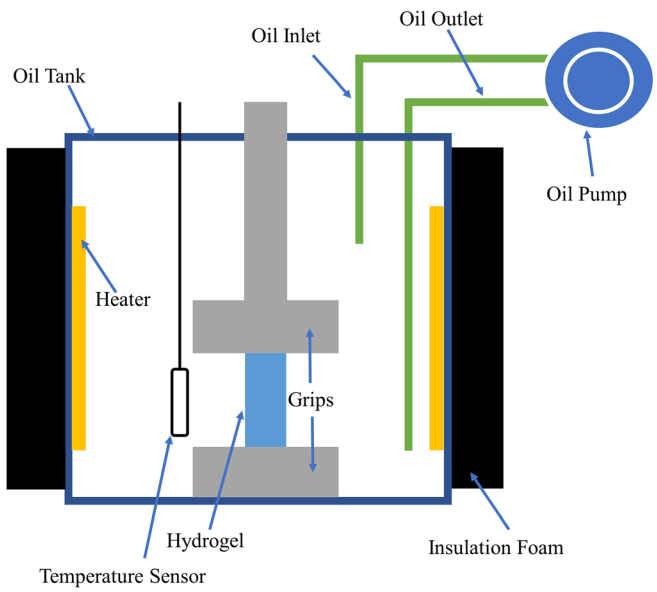

FIG. 1. Schematic view of the experimental setup.

were placed inside the tank to maintain the target temperature. The temperature of the oil near the sample was measured using a digital thermometer (Dallas Semiconductor DS18B20) with $\pm 0.5\,^{\circ}\mathrm{C}$ accuracy. Temperature data were sent to an Arduino board which switched the heater on/off using a simple controller. The control scheme is straightforward: For a target temperature T, we programmed the Arduino controller so that if the temperature was below $T + 0.1\,^{\circ}\mathrm{C}$, the heater would turn on. If the temperature was above $T + 0.3\,^{\circ}\mathrm{C}$, the heater would turn off. Using this method, we were able to hold the temperature within to $\pm 0.5\,^{\circ}\mathrm{C}$ of the target. We also incorporated an oil circulation system which drew the oil from the top of the tank and injected it to the bottom of the tank at a rate of 100 ml/min. This makes the temperature more uniform in the vertical direction. Without the circulation system, we observed up to a $3\,^{\circ}\mathrm{C}$ difference in the temperature between the top and the bottom of the specimen. With oil circulation, we have verified that the temperature difference between the top and the bottom of the sample is less than $1\,^{\circ}\mathrm{C}$. For tests below room temperature, we first cool the oil to the test temperature in a refrigerator and then fill the tank with the cooled oil. As the test progresses, additional cool oil at the test temperature is added. We have verified that by using this method, the temperature change during a 30-min test does not exceed $2\,^{\circ}\mathrm{C}$. It should be noted that for most tests, the testing time was much shorter.

We performed uniaxial tension tests on hydrogel specimens at five different temperatures, 13, 22.5 (defined as room temperature), 30, 40, and $50\,^{\circ}\mathrm{C}$. The specimens were 12 mm in width, 2 mm in thickness, and the initial distance between the grips was 24 mm. At each temperature, we loaded the specimens to a stretch ratio λ of 1.3 at five different stretch rates: 0.001/s, 0.003/s, 0.01/s, 0.03/s, and 0.1/s (except for $13\,^{\circ}\mathrm{C}$ where we tested at four rates excluding 0.003/s). Note that our all tension tests are conducted at constant stretch rates $\dot{\lambda}$ (loading/unloading); thus, since the true strain rate is $\dot{\lambda}/\lambda$, it decreases with the stretch during loading. The unloading rate for all tests was 0.01/s. We also performed stress relaxation tests on these samples at each temperature. In these relaxation tests, we stretched the sample at a fast rate (0.5/s) to a stretch ratio of 1.3 and held the stretch constant for 30 min. We repeated the tests twice at each temperature to check the consistency of the results.

C. Rheology tests

We performed small strain rheology tests using a TA Instruments DHR3 torsional rheometer with parallel plates. Hydrogel sheets with a thickness of 2.1 mm were cut into 20 mm diameter circular specimens using a stainless-steel punch. To eliminate the slip between the specimen and the parallel plates, we applied precompression by setting the gap between the parallel plates to 1.6 mm. We observed that the normal force is constant to within 5% during a cycle and approximately constant over all frequencies (see supplementary material) [16]. No anomalies were seen in the raw or processed data that would suggest slipping. The samples were cyclically loaded to 0.3% strain at frequencies from 0.01 to 10 Hz. To test the limit of linearity, we performed amplitude sweeps and found that the storage and loss modulus data are constant for strains less than 0.3% (see supplementary material). Three data points were taken per decade of frequency. As in the cyclic tension tests, these rheology tests were performed at 13, 22.5, 30, 40, and $50\,^{\circ}\mathrm{C}$. In all tests, the maximum phase angle was less than 40 (see supplementary material). To reduce drying of the gel at elevated temperatures, a solvent trap was used to achieve a high-humidity environment. The trap holds the sample in a small, closed space at close to 100% relative humidity during the tests. We weighed the sample before and after the tests and found that even for the $50\,^{\circ}\mathrm{C}$ tests, the maximum weight loss is less than 5%. The tests were repeated three times to check consistency.

III. RESULTS

A. Uniaxial tension

1. Test results

The nominal stress, σ , versus stretch ratio, λ, curves at different loading rates and temperatures are shown in Figs. 2(a)–2(e). In these figures, the maximum stretch ratio is 1.3 which is considerably higher than typical strains imposed in linear rheology. We have carried test with larger stretch ratios up to 5.5, and these results are reported in earlier works [13]. Even with larger stretch ratios that clearly fall outside the linear regime, our model with strain hardening fits the cyclic test data well with the same set of parameters [13]. During the cycle tests shown here, for all the temperatures and loading rates tested, we found a large hysteresis with a small residual deformation *right after unloading the specimen to zero stress*. At a fixed temperature, the stiffness of the gel increases with the loading rate. This is because the unbroken physical bonds can accumulate more stretch at faster loading rates (see also Sec. IV). Figure 2(f) shows the load versus stretch response at a stretch rate of 0.01/s at different temperatures. The gel is stiffer at a lower temperature and softer at a higher temperature. This behavior can be explained by the kinetics of the physical bonds and will be discussed in Sec. IV.

2. Review of the constitutive model

Our test results can be explained quantitatively by a constitutive model developed in our earlier work [12,13]. Here, we briefly review this constitutive model. Note that the nomenclature here differs slightly from [12] and [13]. Macroscopically, the gel is assumed to be isotropic and incompressible. The model assumes two independent types of bonds: The chemical crosslinks form a permanent elastic network. Physical crosslinks form transient bonds within this network that can break and reattach with rates independent of the stress or strain acting on it. We assume that chemical cross-links do not break. When a strand in the transient network breaks, it instantaneously releases the strain energy it carries. When a broken physical strand reattaches at time τ, it has zero strain energy at that time, even though the

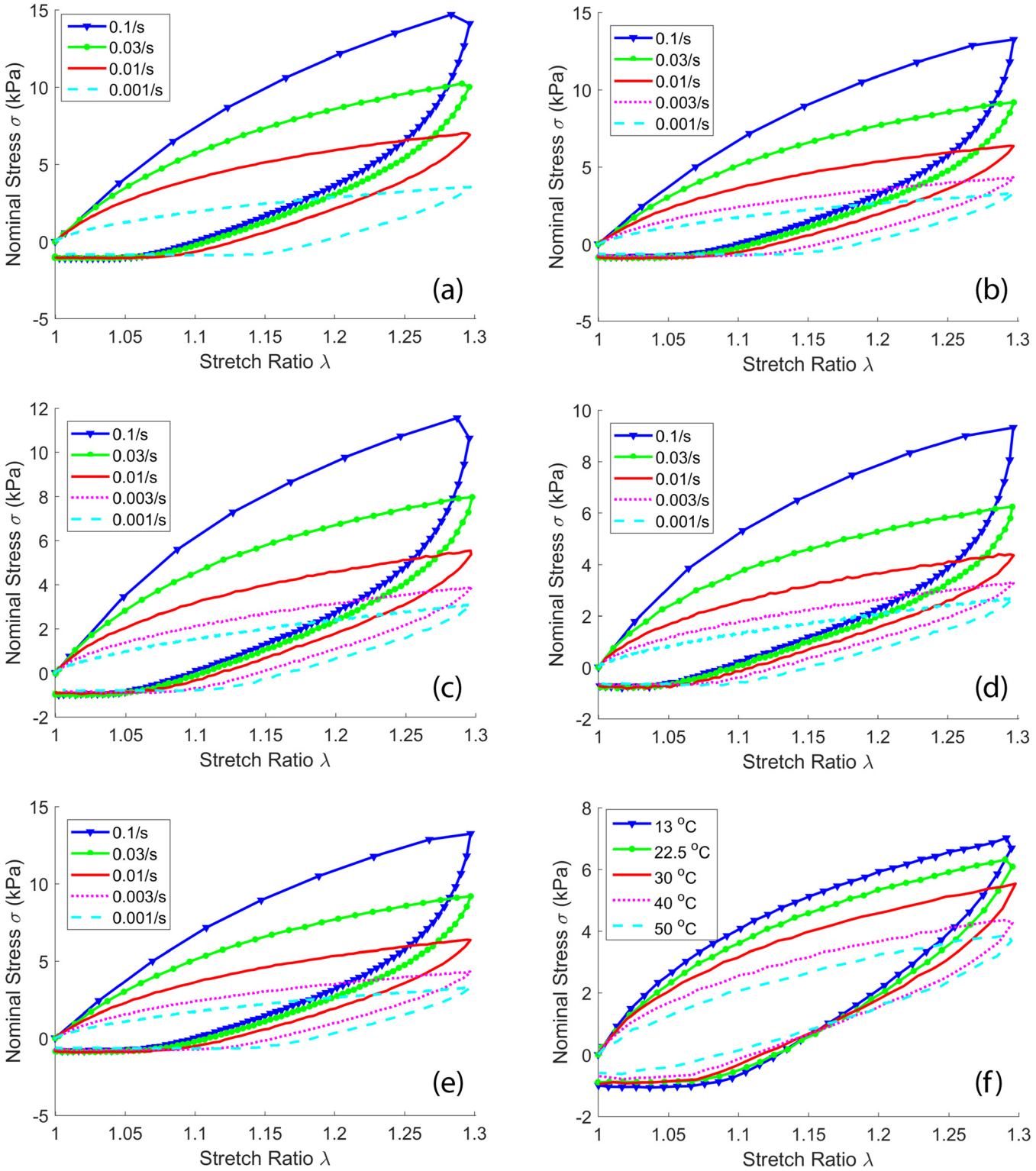

FIG. 2. Uniaxial tension tests data: Nominal stress versus stretch at different stretch rates and temperatures: (a) 13 °C, (b) 22.5 °C, (c) 30 °C, (d) 40 °C, (e) 50 °C, and (f) effects of temperature on the stress-stretch curve at a fixed stretch rate of 0.01/s and varying temperature.

network is strained. The total strain energy is equal to the sum of the strain energy carried by the strands in both networks. We also assume that the breaking and reattaching of the physical strands reaches a dynamic equilibrium soon after the gel is synthesized. This steady state assumption implies that the breaking and reattachment rates are equal and independent of time. This rate is denoted by $\dot{\chi}_\infty$.

As in our previous works, we assume that the strain energy densities of the undamaged networks for both permanent and transient bonds are the same. Since the maximum stretch ratio used in all the experiments reported here is less than or equal to 1.3, strain hardening effects can be neglected, and we use the neo-Hookean strain energy function. With these assumptions, the nominal stress in uniaxial tension is

$$\sigma = G\rho\left[\lambda(t) - \frac{1}{\lambda^2(t)}\right] + Gn(t)\left[\lambda(t) - \frac{1}{\lambda^2(t)}\right] + G\dot{\chi}_\infty \int_0^t \phi_B\left(\frac{t-\tau}{t_B}\right)\left[\frac{\lambda(t)}{\lambda^2(\tau)} - \frac{\lambda(\tau)}{\lambda^2(t)}\right] d\tau, \tag{1a}$$

where G is the small strain shear modulus, ρ is the molar fraction of the chemical crosslinks, and $n(t)$ is the fraction of physical crosslinks that are attached at $t = 0$ and survive until current time $t > 0$ and is given by

$$n(t) \equiv \dot{\chi}_\infty \int_{-\infty}^{0} \phi_B\left(\frac{t-\tau}{t_B}\right) d\tau = \dot{\chi}_\infty \frac{t_B}{2-\alpha_B}\left[1 + (\alpha_B - 1)\frac{t}{t_B}\right]^{\frac{2-\alpha_B}{1-\alpha_B}}. \tag{1b}$$

The "survivability" function ϕ_B

$$\phi_B\left(\frac{t-\tau}{t_B}\right) = \left[1 + (\alpha_B - 1)(t-\tau)/t_B\right]^{1/(1-\alpha_B)} \tag{1c}$$

denotes the fraction of physical crosslinks that are formed at time τ and remain attached at time $t \geq \tau$, where t_B is the characteristic time for breaking and $1 < \alpha_B < 2$ is a material parameter. The dimensionless material parameter α_B controls the average survival time of a newly healed transient bond.

We briefly summarize the physical meaning of Eqs. (1a)–(1c). The first term on the right hand side of Eq. (1a) is the stress carried by the chemical network, the second term represents the loss of stress due to the breaking of the *initially* attached physical strands, while the integral term describes the recovery of stress from the reattachment of physical strands. For example, in a test with continuous loading, the effect of reattachment is to recreate temporary elastic strands attached at both ends but with a different reference configuration than the original chains, which gives rise to the term $\lambda(t)\lambda^{-2}(\tau) - \lambda(\tau)\lambda^{-2}(t)$ in Eq. (1a). This term is consistent with our assumption that the energy of the newly reattached strand carries zero strain energy. Finally, in Eq. (1c), we used a power law function with power exponent α_B to describe the breaking kinetics. This is a phenomenological model motivated by the expectation that there exists a spectrum of relaxation time scales associated with the breaking of physical strands due to the statistical nature in strand life time or the polymer network structure adjacent to a physical strand; empirically, such processes can be well described by power law functions.

Equations 1(a)–1(c) imply that our constitutive model is completely determined by four material parameters: $G\rho$, $G\dot{\chi}_\infty$, α_B, and t_B. These four parameters are determined by a uniaxial relaxation test where we first load a sample at a constant stretch rate to a fixed stretch ratio, then hold it at this stretch until the stress reaches a plateau. The plateau stress, the log–log plot of the stress vs time at large time (use both the slope and the intercept from the linear fit), and the initial slope of the loading part provide us four conditions for the four material parameters, so that the material parameters can be estimated. Then, the parameters can be iterated to give the best fit to loading/unloading tests carried out at constant stretch rates. Further details of the model identification procedure are described in our previous work [13]. In [13], we have shown that $\dot{\chi}_\infty$ depends on t_B as well as the characteristic healing time of physical bond t_H by

$$\dot{\chi}_\infty = \frac{1-\rho}{t_H + \frac{t_B}{2-\alpha_B}};$$

hence $\dot{\chi}_\infty$ is expected to be temperature dependent.

3. Determination of material parameters and comparison to experiments

Previously, we have shown that our constitutive model is able to accurately predict uniaxial tension test data at room temperature [12,13]. Here, we demonstrate that it can also accurately predict the uniaxial tension tests at different temperatures. For each temperature, we first use the stress relaxation test data to estimate the four material parameters (details of method of fitting were given in our previous paper [13]). These parameters are then fine-tuned to match both the cyclic tension test data and the rheology data (see Sec. III B) and are summarized in Table I. It can be seen that temperature has different effects on these four parameters. The parameters $G\rho$ and α_B are insensitive to temperature, while $G\dot{\chi}_\infty$ increases and t_B decreases with increasing temperature.

Next, we use these parameters to predict the stress-stretch curve for the uniaxial constant stretch rate tension tests (see Sec. III A 1) and compare these predictions with test data. Figures 3(a)–3(c) compare model predictions with experiments for three temperatures and three loading rates, and Fig. 3(d) shows the comparison to relaxation test data for the three temperatures. There is excellent agreement between model predictions and experimental data. The results for the other temperatures and stretch rates are just as good and are given in the supplementary material.

B. Rheology

1. Experimental data and shifting

The storage modulus G', loss modulus G'', and $\tan\delta = G''/G'$ obtained from rheology tests at linear-viscoelastic region are shown in Figs. 4(a)–4(c). First, we investigate whether these data can be collapsed into a single master curve

TABLE I. Model fitting parameters.

Temperature (°C)	$G\rho$ (kPa)	$G\dot{\chi}_\infty$ (kPa/s)	α_B	t_B (s)	$\frac{G\dot{\chi}_\infty t_B}{2-\alpha_B}$ (kPa)
13	3.34	25.21	1.62	0.49	32.62
22.5	3.14	27.85	1.62	0.42	30.94
30	3.33	34.30	1.62	0.32	28.85
40	3.11	46.12	1.61	0.21	25.15
50	3.16	53.60	1.61	0.16	22.55

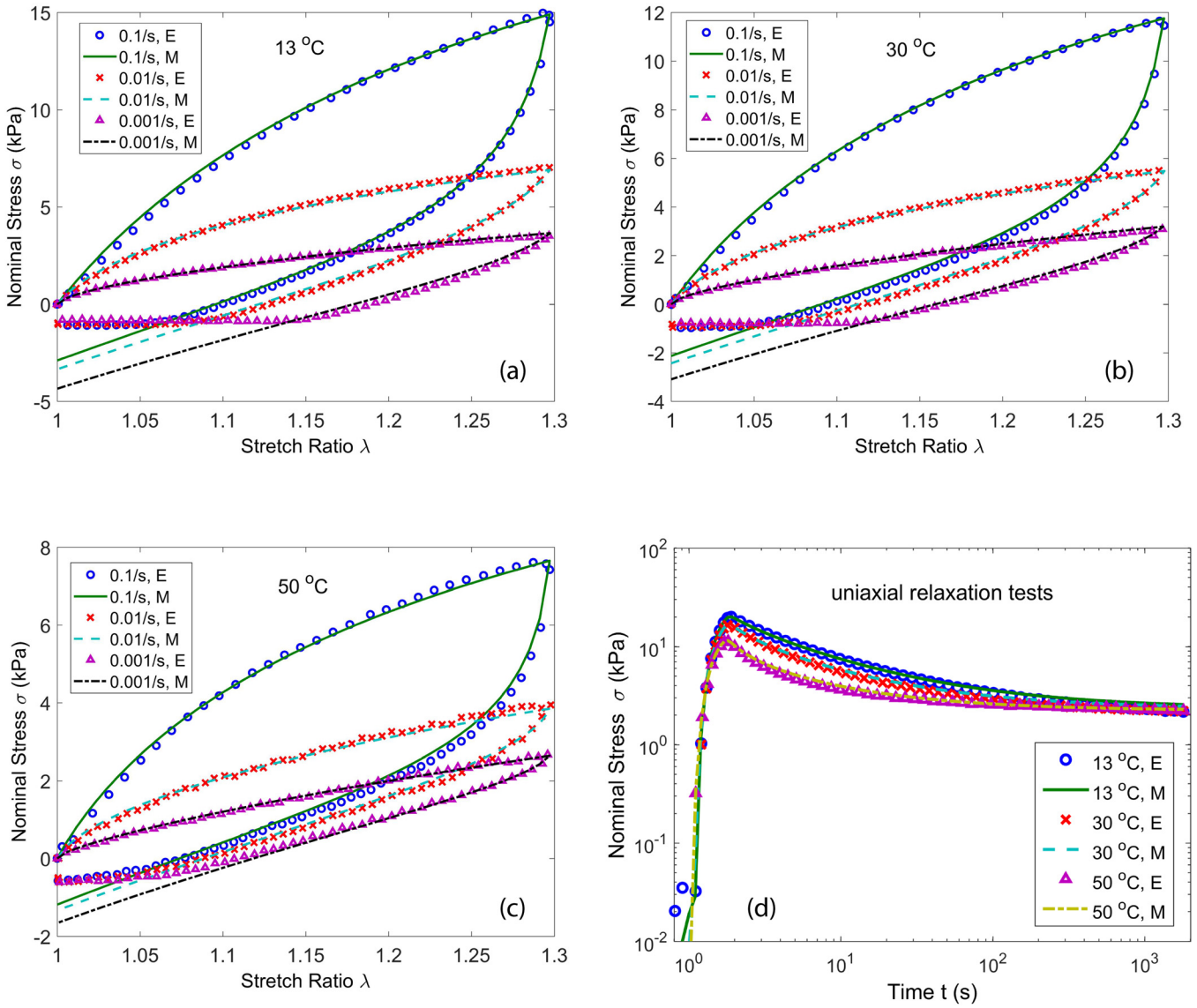

FIG. 3. Comparison of model and experimental tests at three different stretch rates and temperatures of (a) 13 °C, (b) 30 °C, and (c) 50 °C, and (d) is the comparison of model and experimental tests for the above three tests for relaxation test, where the sample is first loaded at a constant stretch rate to a stretch ratio at 1.3 then held at this stretch. "E" stands for experimental data and "M" stands for model prediction using parameters from Table I. In the experiments, samples are unloaded to zero stretch, therefore, some samples go into compression and buckle. The model calculation does not account for buckling.

using TTS [17] defined by $b_T G'(T, \omega a_T) = G'(T_{Ref}, \omega)$, where ω is the frequency, T is temperature, and a_T and b_T are the horizontal and vertical shift factors. The same shifting is applied to G''. We use room temperature $T_{Ref} = 22.5\,^{\circ}\mathrm{C}$ as the reference temperature. In conventional polymer melts where the dynamics is due to monomer friction, *tan* δ data at different temperatures depend only the horizontal shift factor a_T, because both G' and G'' are affected by the same vertical shift factor. Thus, we first use the *tan* δ data to obtain the horizontal shift factors at each temperature. The shifted *tan* δ data are plotted in Fig. 5(a). We apply these horizontals shifts to G' followed by a vertical shift to collapse these data onto a master curve. The same vertical shift is then applied to G''. The results are shown in Figs. 5(b) and 5(c). The shift factors are tabulated in Table II. Comparing Figs. 5(a)–5(c) with the pre-shifted data in Figs. 4(a)–4(c), we conclude that the TTS works well for our gel for all the frequencies in the tests. The horizontal shift factors have a wide range, from 1.20 to 0.41 over the 13–50 °C temperature range, while the vertical shift has a smaller range, 0.96–1.16.

2. G′ and G″ from constitutive model

In our previous work [14], we derived G', G'' based on our constitutive model

$$G'(\omega) = G\rho + G\rho K(T) I_1(\omega t_B, \alpha_B), \tag{2a}$$

$$G''(\omega) = G\rho K(T) I_2(\omega t_B, \alpha_B), \tag{2b}$$

where

$$I_1(\omega t_B, \alpha_B) \equiv 1 - \frac{2-\alpha_B}{\alpha_B - 1} \int_0^{\infty} \cos\left(\frac{\omega t_B}{\alpha_B - 1} x\right) (1+x)^{-\frac{1}{\alpha_B - 1}} dx, \tag{2c}$$

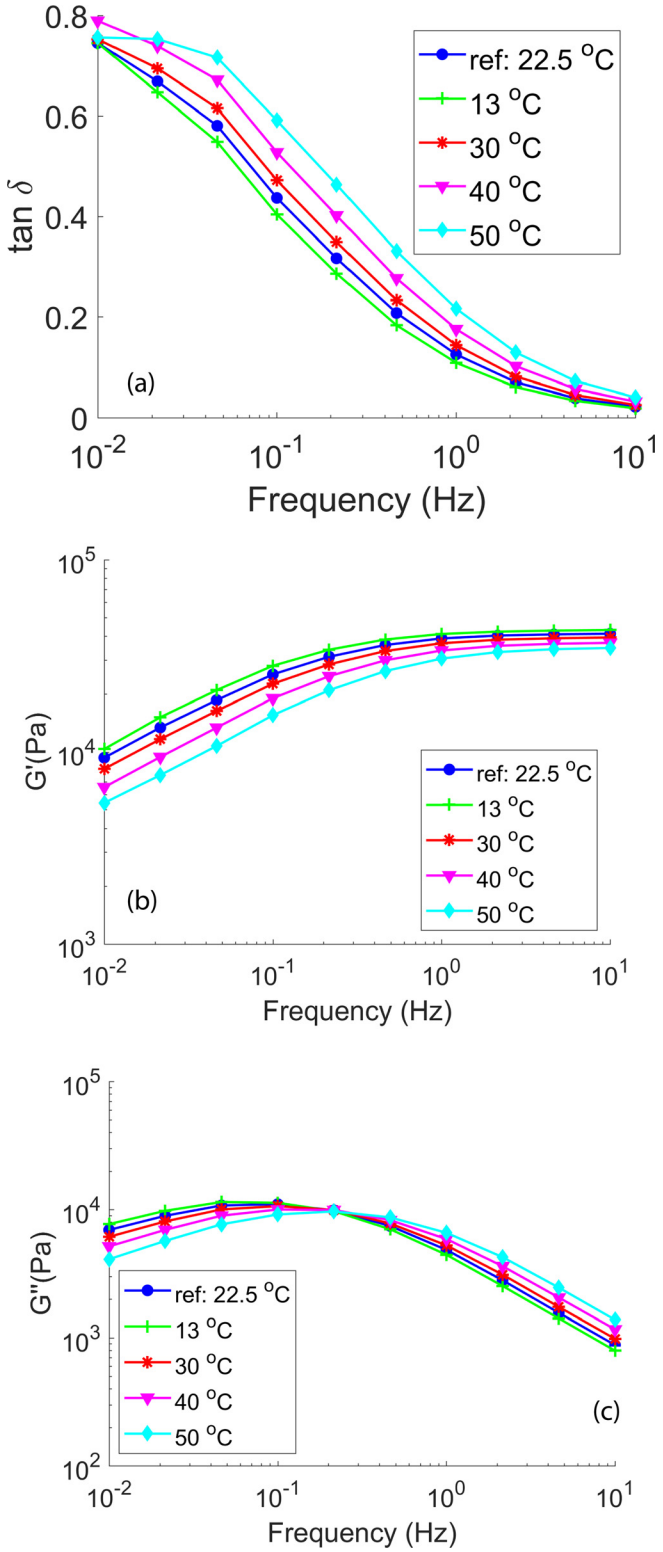

FIG. 4. Rheology test results: (a) tan δ, (b) G', and (c) G''.

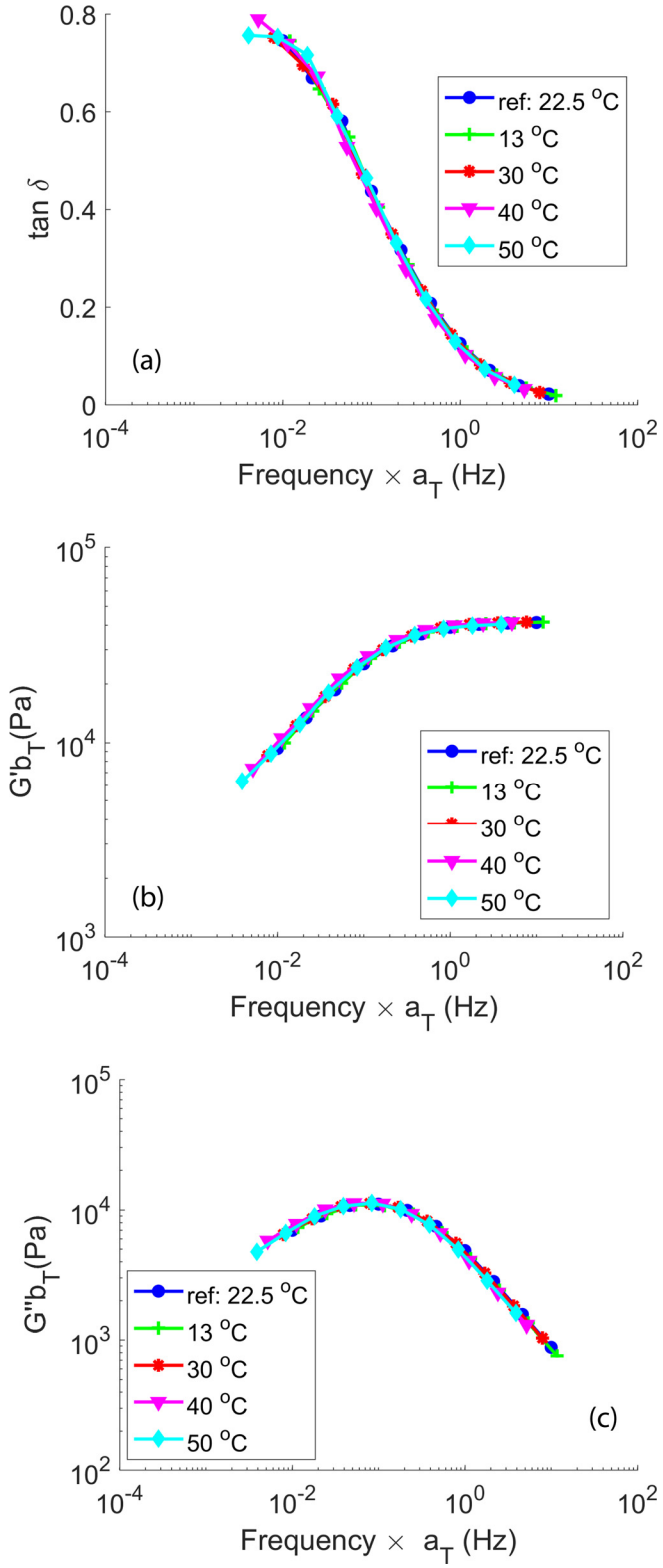

FIG. 5. Master curves of: (a) *tan* δ, (b) G', and (c) G''.

$$I_2(\omega t_B, \alpha_B) \equiv \frac{2-\alpha_B}{\alpha_B - 1} \int_0^\infty \sin\left(\frac{\omega t_B}{\alpha_B - 1} x\right)(1+x)^{-\frac{1}{\alpha_B - 1}} dx, \quad \text{(2d)}$$

$$K(T) = \frac{\dot{\chi}_\infty t_B}{(2-\alpha_B)\rho} = \frac{(1-\rho)/\rho}{1 + (2-\alpha_B)(t_H/t_B)}, \quad \text{(2e)}$$

where ω is the frequency in rad/s. Using the parameters listed in Table I, we can also calculate the storage modulus G', loss modulus G'', and $\tan\delta = G''/G'$ in the rheology tests. Comparison between the model and the experiment at room temperature is shown in Fig. 6. The model agrees well with the experimental data. Results for other temperatures fit equally well and are shown in the supplementary material.

TABLE II. Shift parameters from model fitting and rheology results.

Temperature (°C)	t_B	a_T from tension tests	a_T from rheology	b_T from tension tests	b_T from rheology
13	0.49	1.17	1.20	0.95	0.96
22.5 (ref.)	0.42	1.00	1.00	1.00	1.00
30	0.32	0.77	0.79	1.07	1.05
40	0.22	0.52	0.53	1.23	1.12
50	0.16	0.39	0.41	1.37	1.16

IV. DISCUSSION OF RESULTS

A. Time temperature superposition

In Sec. III, we showed that the uniaxial cyclic test data at different temperatures and loading rates are captured well by our constitutive model. There are four independent material parameters in our model, and they are given in Table I for different temperatures. In a stress relaxation test, the modulus at long time is $G\rho$. Here, ρ is the molar fraction of chemical crosslinks, which we do not expect to have a strong temperature dependence. The small strain shear modulus G is, according to rubber elasticity, proportional to the absolute temperature, so the fractional change in $G\rho$ should be very small for the range of temperature used in our experiments. This is consistent with the results of our relaxation test which shows that the long time moduli are quite insensitive to temperature (see supplementary material).

The other two material parameters, $G\dot{\chi}_\infty$ and t_B, describe the dynamics of chain breaking and reattaching. As the temperature increases, the dynamics accelerate, resulting in a shorter average chain life; thus, one would expect the characteristic time for breaking, t_B, to decrease with temperature. Finally, Table I shows that the exponent α_B of the survivability function ϕ_B is insensitive to temperature.

To make further contact with our model, consider the storage modulus G' and loss modulus G'' given in Eqs. (2a)–(2d). In order for TTS to work *perfectly*, G' and G' should have the separable form as given below

$$G' = b(T)\phi_S(\omega a(T)), \tag{3a}$$

$$G'' = b(T)\phi_L(\omega a(T)), \tag{3b}$$

$$\Rightarrow \tan\delta = \phi_L(\omega a(T))/\phi_S(\omega a(T)), \tag{3c}$$

where $b(T)$ and $a(T)$ are functions that depend *only* on temperature T, ϕ_S and ϕ_L are functions that depends *only* on the combination $\omega a(T)$. In Eqs. (3a) and (3b), $b(T)$ and $a(T)$ are responsible for vertical and horizontal shifts, respectively. Since ω appears only in the factor ωt_B in $I_1(\omega t_B, \alpha_B)$ and $I_2(\omega t_B, \alpha_B)$ [see Eqs. (2a)–(2d)], t_B can be identified with $a(T)$ and the horizontal shift as long as α_B is *independent of temperature*. Our results in Table I support this feature of our model. Next, consider the $\tan\delta = G''/G'$ obtained by dividing Eq. (2b) by Eq. (2a), it is

$$\tan\delta = \frac{K(T)I_2(\omega t_B)}{1 + K(T)I_1(\omega t_B)}, \tag{4}$$

where we have excluded α_B from the argument of I_1 and I_2 since it is found to be independent of temperature. Equation (4) implies that $\tan\delta$ is independent of the vertical shift if and only if $K(T) = K_0$ is independent of temperature. Indeed, if this is the case, then the storage and loss moduli have the same form as Eqs. (3a) and (3b), i.e.,

$$G' = \underbrace{G\rho K_0}_{b(T)} \underbrace{\left[\frac{1}{K_0} + I_1(\omega t_B)\right]}_{\phi_S(\omega t_B)}, \quad G'' = \underbrace{G\rho K_0}_{b(T)} \underbrace{[I_2(\omega t_B)]}_{\phi_L(\omega t_B)}. \tag{5}$$

From Eq. (5), we see that $G\rho K_0 = b(T)$ and is given by

$$G\rho K_0 = \frac{G\dot{\chi}_\infty t_B}{2 - \alpha_B} = b(T). \tag{6}$$

In the following, we identify the vertical and horizontal shift factors as $b_T(T) \equiv b(T)/b(T_0)$ and $a_T(T) \equiv a(T)/a(T_0)$, respectively.

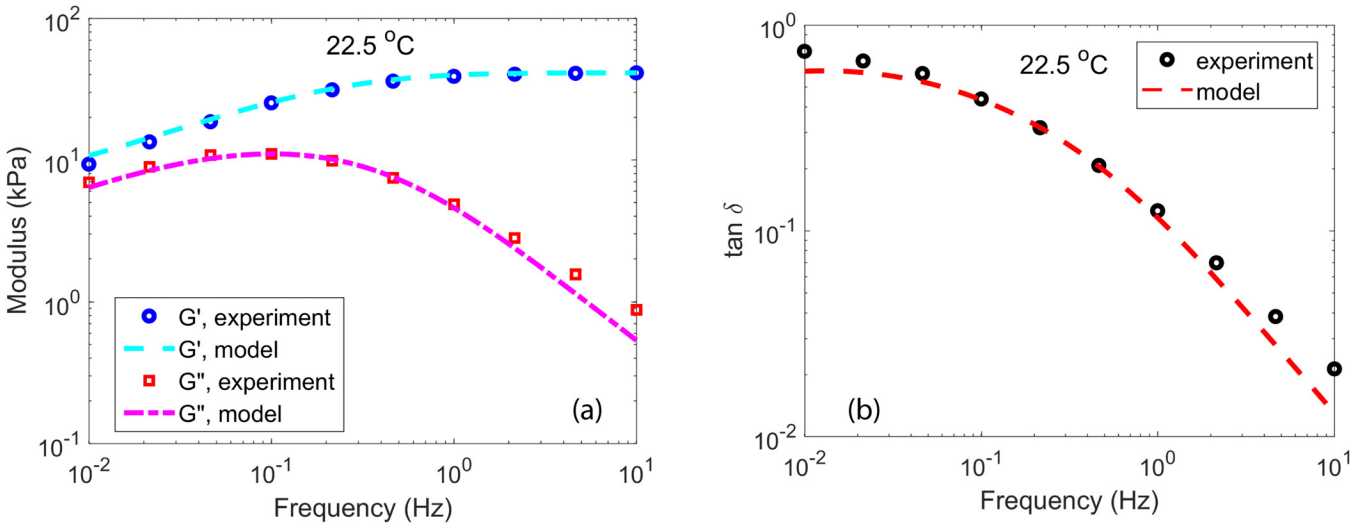

FIG. 6. G', G'', and *tan* δ at room temperature. (a) G' and G'' evaluated using Eqs. (2a) and (2b) and parameters from Table I with rheology data (model results are shifted by a vertical constant to account for precompression, this procedure was also used in our previous work). (b) *tan* δ from model and rheology data.

In the constitutive model, t_B, the characteristic breaking time in the survivability function decreases with temperature as a result of accelerated breaking kinetics. As Eqs. 2(a) and 2(b) show, the frequency and temperature dependence are given by the product ωt_B. Since the frequency is the inverse of time, a_T should be given by t_B/t_B^{Ref}, where t_B^{Ref} is the breaking time at a reference temperature (room temperature for our case). Using the breaking times, we obtained from the tension tests, we can compute the shift factor t_B/t_B^{Ref} and compare these with the shift factors obtained from rheology test. We also compare the vertical shift factor computed using Eq. (6) from rheology and tension data. These comparisons are shown in Table II and Fig. 7. It can be seen that the horizontal factors computed from both sources are highly consistent. The vertical shift factors agree less well at the higher temperatures (40 and 50 °C). This is because $K(T)$ is not a constant independent of temperature. From Eq. (2e), $K(T)$ depends on ρ and on the ratio t_H/t_B. This ratio need not be independent of temperature since the characteristic time of healing t_H depends on the availability of binding sites, which is not the case for breaking. In addition, since the number of "free" physical crosslinkers which are not bound to the network increases with temperature, the molar fraction of the chemical crosslinks ρ could increase with temperature. For this reason, we cannot expect $K(T)$ to be independent of temperature, and therefore, TTS is not completely satisfied by our model. Indeed, the last column of Table I shows that $K(T)$ decreases very slowly for the first three temperatures but decreases somewhat faster at higher temperatures.

Finally, our data suggest that $\log a_T$ and $\log(1/(b_T T))$ are approximately inversely linear in temperature, i.e.,

$$\log(a_T) = \frac{E_a}{2.303R}\left(\frac{1}{T} - \frac{1}{T_0}\right), \tag{7a}$$

$$\log\left(\frac{1}{Tb_T}\right) = \frac{E_b}{2.303R}\left[\frac{1}{T} - \frac{1}{T_0}\right], \tag{7b}$$

where $R = 8.314$ J/mol K is the gas constant, E_a and E_b are the activation energies associated with bond breaking and the enthalpy of association, respectively. Figures 7(a) and 7(b) compare Eqs. (7a) and (7b) with the shift factors we obtained from rheology test and tension test data, using $E_a = 25.6$ kJ/mol and $E_b = 6.63$ kJ/mol. Within the range of temperatures considered here, the shift factors fit the Arrhenius law, Eqs. (7a) and (7b), well with some deviation at low temperature. The value of E_a is reasonable for a PVA-borax system; for solutions (without chemical crosslinks), a value of 42 kJ/mol was previously reported [18,19]. The value of E_b is much smaller than E_a which is to be expected since the vertical shift is much less. This is the reason why TTS works in this frequency range. We expect TTS to break down at very low frequencies when the gel is elastic and dominated by chemical cross-linking.

B. Applicability and limits of model

The constitutive model was developed specifically for PVA gels with a fixed composition of chemical and physical cross-links. Recently, we have varied these compositions and found that our model works just as well. Hence, we expect our model should work well for other gels with chemical and physical cross-links. However, the key assumption that the breaking and healing kinetics of physical bonds are independent of the stress acting on these bonds will limit its applicability. Preliminary work in our group shows that by modifying our model such that the survivability function in Eq. (1c) depends on stress we are able to predict the mechanical behavior of the tough, polyampholyte gels of Gong *et al.* [1].

The model is not expected to apply to purely physical gels (associative polymer solutions) in a long time range and/or at a high strain, because the model does not take into account of the terminal dynamics of the polymer chains. For purely chemical gels, the model reverts to a simple Neo-Hookean material, which works reasonably well for the corresponding chemical gel.

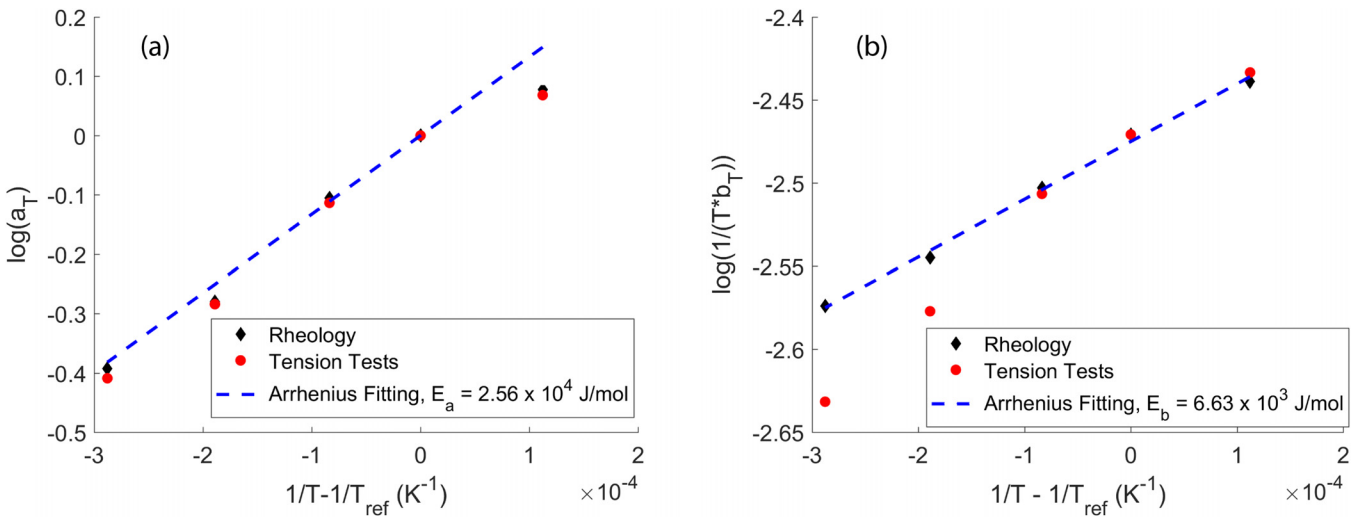

FIG. 7. (a) Horizontal shift factors: $\log_{10} a_T$ from the rheology tests, calculated from the tension tests and from Arrhenius fitting of the shift factors, using $E_a = 2.56 \times 10^4$ J/mol. (b) Vertical shift factors: $\log_{10} b_T$ from the rheology tests, calculated from the tension tests and from Arrhenius fitting of the shift factors, using $E_b = 6.63 \times 10^3$ J/mol.

V. SUMMARY AND CONCLUSIONS

Cyclic tension and rheology tests are carried out on a PVA dual cross-link hydrogel at different temperatures. The tension tests are performed under moderately large strains, while the rheology tests are performed at small strains. The storage and loss moduli from the rheology tests are found to obey TTS. Model parameters from large strain tests of one batch of material are found to accurately predict the small strain rheology results from a second match of the material.

Of considerable significance is that the tension cyclic test and rheology test data at all test temperatures can be explained by a nonlinear viscoelastic constitutive model with four independent material parameters $\{G\rho, G\dot{\chi}_\infty, \alpha_B, t_B\}$. These parameters are determined independently by performing relaxation tests at different temperatures and after a slight amount of fine-tuning are found to match both tension and rheology data at different temperatures. We find that α_B and $G\rho$ are approximately independent of temperature, while $G\dot{\chi}_\infty$ and t_B are strongly temperature dependent. It should be noted that TTS imposes very stringent requirements on our constitutive model. We find that the constitutive model approximately satisfies the stringent requirements needed for simple TTS to be valid.

In summary, our constitutive model is capable of quantifying complex loading histories in uniaxial tension test and at the same time correctly captures linear rheology of a PVA dual-crosslinked hydrogel at different temperatures. The general framework of the constitutive model is applicable to other gels with chemical and physical cross links. When no physical crosslinks are present the model reverts to a simple Neo-Hookean material, which works reasonably well for the corresponding chemical gel. The model is not expected to capture the behavior of a purely physical gel.

ACKNOWLEDGMENTS

J.G., M.L., C.Y.H., and A.Z. are supported by the National Science Foundation under Grant No. CMMI-1537087. This work made use of the Cornell Center for Materials Research Shared Facilities, which are supported through the NSF MRSEC Program (No. DMR-1719875). The authors thank an anonymous reviewer for asking us to check the limit of linear rheology.

References

[1] Gong, J. P., Y. Katsuyama, T. Kurokawa, and Y. Osada, "Double-network hydrogels with extremely high mechanical strength," Adv. Mater. **15**, 1155–1158 (2003).

[2] Okumura, Y., and K. Ito, "The polyrotaxane gel: A topological gel by figure-of-eight cross-links," Adv. Mater. **13**, 485–487 (2001).

[3] Sakai, T., T. Matsunaga, Y. Yamamoto, C. Ito, R. Yoshida, S. Suzuki, N. Sasaki, M. Shibayama, and U. Chung, "Design and fabrication of a high-strength hydrogel with ideally homogeneous network structure from tetrahedron-like macromonomers," Macromolecules **41**, 5379–5384 (2008).

[4] Sun, J.-Y., X. Zhao, W. R. K. Illeperuma, O. Chaudhuri, K. H. Oh, D. J. Mooney, J. J. Vlassak, and Z. Suo, "Highly stretchable and tough hydrogels," Nature **489**, 133–136 (2012).

[5] Webber, R. E., C. Creton, H. R. Brown, and J. P. Gong, "Large strain hysteresis and mullins effect of tough double-network hydrogels," Macromolecules **40**, 2919–2927 (2007).

[6] Zhang, W., X. Liu, J. Wang, J. Tang, J. Hu, T. Lu, and Z. Suo, "Fatigue of double-network hydrogels," Eng. Fracture Mech. **187**, 74–93 (2018).

[7] Sun, T. L., T. Kurokawa, S. Kuroda, A. Bin Ihsan, T. Akasaki, K. Sato, Md. A. Haque, T. Nakajima, and J. P. Gong, "Physical hydrogels composed of polyampholytes demonstrate high toughness and viscoelasticity," Nat. Mater. **12**, 932–937 (2013).

[8] Zhao, X., "Multi-scale multi-mechanism design of tough hydrogels: Building dissipation into stretchy networks," Soft Matter **10**, 672–687 (2014).

[9] Creton, C., "50th anniversary perspective: Networks and gels: Soft but dynamic and tough," Macromolecules **50**, 8297–8316 (2017).

[10] Sun, T. L., F. Luo, W. Hong, K. Cui, Y. Huang, H. J. Zhang, D. R. King, T. Kurokawa, T. Nakajima, and J. P. Gong, "Bulk energy dissipation mechanism for the fracture of tough and self-healing hydrogels," Macromolecules **50**, 2923–2931 (2017).

[11] Mayumi, K., A. Marcellan, G. Ducouret, C. Creton, and T. Narita, "Stress–strain relationship of highly stretchable dual cross-link gels: Separability of strain and time effect," ACS Macro Lett. **2**, 1065–1068 (2013).

[12] Long, R., K. Mayumi, C. Creton, T. Narita, and C.-Y. Hui, "Time dependent behavior of a dual cross-link self-healing gel: Theory and experiments," Macromolecules **47**, 7243–7250 (2014).

[13] Guo, J., R. Long, K. Mayumi, and C.-Y. Hui, "Mechanics of a dual cross-link gel with dynamic bonds: Steady state kinetics and large deformation effects," Macromolecules **49**, 3497–3507 (2016).

[14] Long, R., K. Mayumi, C. Creton, T. Narita, and C.-Y. Hui, "Rheology of a dual crosslink self-healing gel: Theory and measurement using parallel-plate torsional rheometry," J. Rheol. **59**, 643–665 (2015).

[15] Zhao, J., K. Mayumi, C. Creton, and T. Narita, "Rheological properties of tough hydrogels based on an associating polymer with permanent and transient crosslinks: Effects of crosslinking density," J. Rheol. **61**, 1371–1383 (2017).

[16] See supplementary material at https://doi.org/10.1122/1.5029466 for data and model fits for data and fits of cyclic loading, relaxation loading, and torsional rheometry at all temperatures, results of the amplitude sweep and the normal force measurements in the rheometry tests.

[17] Dealy, J., and D. Plazek, "Time-temperature superposition—A users guide," Rheol. Bull. **78**, 16–31 (2009).

[18] Narita, T., and T. Indei, "Microrheological study of physical gelation in living polymeric networks," Macromolecules **49**, 4634–4646 (2016).

[19] Schultz, R., and M. Raymond, "The chemorheology of poly(vinyl alcohol)–Borate gels," Macromolecules **2**, 281–285 (1969).